Chapter 3

A theoretical analysis of the chiral structures formed by the smectic-C liquid crystal domains

3.1 Introduction

In this chapter, we present a theoretical analysis of the stability of the chiral domain structure described in the previous chapter. We show that the chiral symmetry breaking is due to a combination of surface anchoring and bulk elastic properties specific to smectic-C liquid crystals. In particular, a cross-coupling between the twist and bend distortions in the c-vector field is responsible for the helical structure of these domains. This is the *first demonstration* of the effect of such a coupling which is permitted by the symmetry of smectic-C liquid crystals. The sign and magnitude of the corresponding elastic constant are estimated by comparing the theoretical results with the experiments. We have also analysed the effect of the twist-bend coupling on the stability of a straight $+2$ disclination line. It is shown that the line prefers to be tilted with respect to the smectic layer normal. As mentioned in the previous chapter, the SmC domains produce a twist distortion in the surrounding nematic. An estimate of this twist distortion energy shows that it increases rapidly as the domain diameter approaches the cell thickness. An analysis of the domain shape taking this elastic distortion and the anisotropy in the interfacial tension into account shows that the equilibrium shape is highly anisotropic. Also, as the volume of the domain is increased, the domain length increases much more rapidly than the

radius, which is in accord with the experimental observations.

Before going into the details of the calculations, we give a brief introduction to the theory of elasticity of SmC liquid crystals.

3.1.1 Elastic properties of smectic-C

As already mentioned in the first chapter, smectic liquid crystals have a crystalline order along one direction and a liquid-like order in the orthogonal directions. Moreover, there is an orientational ordering of the molecules within the layers. Thus they can exhibit both 'crystal-like' and curvature elastic properties. In smectic-A, 'a small distortion of the layer spacing (compression or dilation) creates an energy density proportional to $(\nabla_z u)^2$, where u describes the displacement field (Hooke's law). Similarly, layer curvatures not involving any change in the distance between the layers will cost an energy proportional to $(\nabla_{\perp}^2 u)^2$ due to the splay distortion of the Frank-director (note: in SmA, the Frank-director is parallel to the layer normal). In the case of smectic-C , there is an additional degree of freedom, namely, the orientation of the c-vector. The c-vector can have splay, bend and twist distortions like the Frank-director in nematics. But the c-vector is polar unlike the Frank-director which is apolar. The magnitude of the elastic constant corresponding to layer spacing variations is estimated to be around $10^8 erg\,cm^{-3}$. Although this is small compared to that for crystals $(\sim 10^{10} erg\,cm^{-3})$, the layer spacing variations are energetically very expensive compared to pure curvature distortions. The elastic constant corresponding to the curvature distortions is $\sim 10^{-6} dyne$. Therefore, in many situations, it is a good approximation to assume that the layer spacing is constant.

The smectic-C free energy density should be invariant under the transformations of the C_{2h} symmetry group which are the following:

- Reflection about a plane containing the layer normal, N and c.

- Two-fold rotations about an axis perpendicular to N and c. We represent this axis by $\mathbf{p} = \hat{\mathbf{N}} \times \mathbf{c}$.

Also, the energy should remain invariant under global rotations and translations. The bulk curvature elastic free energy density of an incompressible SmC can then be written as [35]

$$
\begin{aligned}
f_{el}^{SmC} = \quad & \frac{K_4}{2}(\mathbf{\nabla} \cdot \hat{\mathbf{N}})^2 + \frac{K_5}{2}(\mathbf{p} \cdot \mathbf{\nabla} \times \mathbf{c})^2 + K_6(\mathbf{\nabla} \cdot \hat{\mathbf{N}})(\mathbf{p} \cdot \mathbf{\nabla} \times \mathbf{c}) \\
& + \frac{K_b}{2}(\hat{\mathbf{N}} \cdot \mathbf{\nabla} \times \mathbf{c})^2 + \frac{K_s}{2}(\mathbf{\nabla} \cdot \mathbf{c})^2 + \frac{K_t}{2}(\mathbf{c} \cdot \mathbf{\nabla} \times \mathbf{c})^2 \\
& + K_{bt}(\hat{\mathbf{N}} \cdot \mathbf{\nabla} \times \mathbf{c})(\mathbf{c} \cdot \mathbf{\nabla} \times \mathbf{c}) + K_7(\mathbf{\nabla} \cdot \mathbf{c})(\mathbf{p} \cdot \mathbf{\nabla} \times \mathbf{c}) \\
& + K_8(\mathbf{\nabla} \cdot \hat{\mathbf{N}})(\mathbf{\nabla} \cdot \mathbf{c}) \, .
\end{aligned} \tag{3.1}
$$

For SmC , the layer curvature energy is anisotropic. The elastic modulus for curvatures in the $N - c$ plane is different in magnitude from that for curvatures in the perpendicular plane. The first term in Eq. 3.1 is the isotropic part of the layer curvature energy. The second term gives the anisotropic contribution. Terms with coefficients K_5, K_6, K_7 and K_8 occur due to the coupling between layer curvature and c-field distortions. The terms with constants K_b, K_s and K_t describe the bend, splay and twist deformations in the c-field, respectively, and are the three principal deformations of the c-field, not involving layer distortions. The term with K_{bt} is a coupling between the bend and twist deformations in the c-field. In the next section we show that it is this coupling that is responsible for the helical nature of the chiral domains.

No *chiral (pseudoscalar)* terms are allowed in the free energy expression by the C_{2h} symmetry of the SmC layers. This is not the case if chiral molecules are added to a SmC liquid crystal. In such chiral systems, the point symmetry of the layers is reduced to C_2, and hence chiral terms can be included as we shall see in the fifth chapter, Sec. **5.2.3.**

3.2   Stability analysis of the chiral domain structure

In this section, we calculate the elastic energy of the SmC domain and show that with the bent c-field configuration described in the previous chapter within each layer, the elastic free energy is indeed minimised for a helical stacking of such layers. To simplify the analysis we make the following assumptions:

- We assume that there is no compressive or dilative distortion of the smectic layers. This assumption is based on the following argument. Consider a SmC domain of size L. Layer dilation/compression elastic energy scales as $B(\nabla_z u)^2 L^3 \sim B\zeta^2 L^3$, where B is the relevant elastic constant. Similarly, distortions in the c-field cost energies which scale as $(K/L^2)L^3$. For these two contributions to be comparable, $\zeta \sim (K/B)^{1/2}(1/L) = \lambda/L$, where X is of the order of molecular dimensions. Therefore, λ/L has to be negligibly small if the two energies are to be comparable. In other words, layer spacing variations are energetically very expensive compared to curvature distortions.

- The experiments described in the previous chapter indicate that the SmC layers are flat. Therefore, terms describing layer curvatures can be dropped from Eq. **3.1.**

- We assume strong 'anchoring' of the molecules at the $N\text{-}SmC$ interface and assume that the singularity lies on the surface of the domain (the effect of relaxing this condition will be discussed later). This allows us to calculate the contributions to the total elastic energy from the smectic domain and the surrounding nematic independently.

- The analysis is for long domains in which the elastic energy contribution from the tips can be ignored compared to that from the bulk and the domains can be considered as perfectly cylindrical. Experimentally, domains as long as
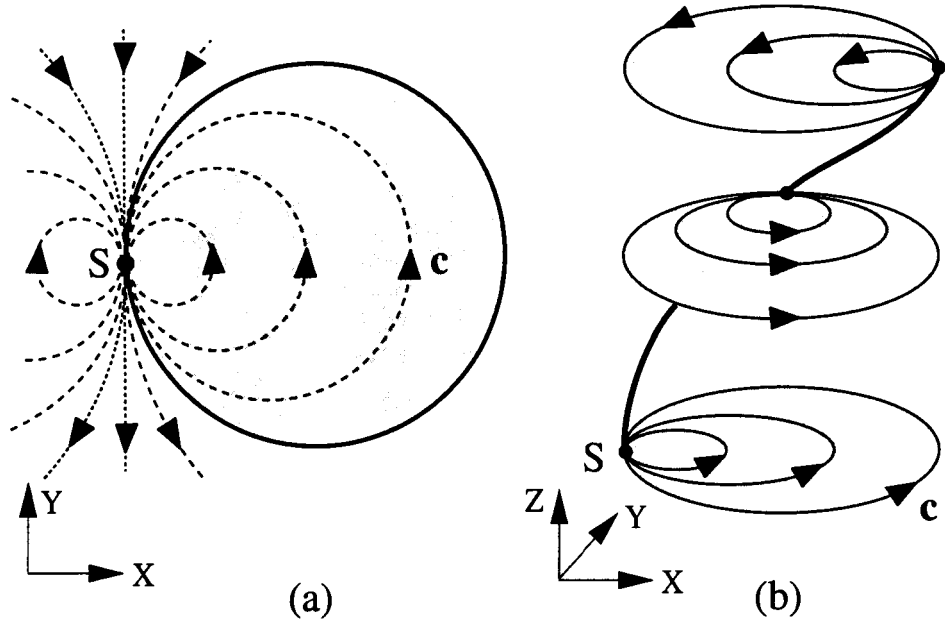
Figure 3.1: (a) The c-field within each SmC layer (shaded region) can be considered as a part of a $+2$ disclination (dashed curves). (b) The pattern in (a) rotates from layer to layer to produce a helical structure. Three typical layers within half a pitch of the helix are shown.

---

be along the X-axis, Eq. 3.4 reduces to

$$f_{el}^{SmC} = \frac{K}{2}(\nabla_x \phi)^2 + \frac{K_t}{2}(\nabla_z \phi)^2 - K_{bt}(\nabla_x \phi)(\nabla_z \phi) , \tag{3.5}$$

which is in a form originally written by the Orsay group [37]. The free energy density (Eq. 3.5) can be written in the form

$$f_{el}^{SmC} = (\nabla_i \phi) K_{ij} (\nabla_j \phi) \quad ; i, j = x, z , \tag{3.6}$$

where

$$K_{ij} = \begin{bmatrix} K & K_{bt} \\ K_{bt} & K_t \end{bmatrix} ,$$

is a real symmetric matrix. The stability condition is given by $K > 0$, $K_t > 0$, and $det[K_{ij}] > 0$ (which implies $KK_t - K_{bt}^2 > 0$).

The Euler-Lagrange equation corresponding to Eq. 3.4, assuming a one elastic constant approximation, is

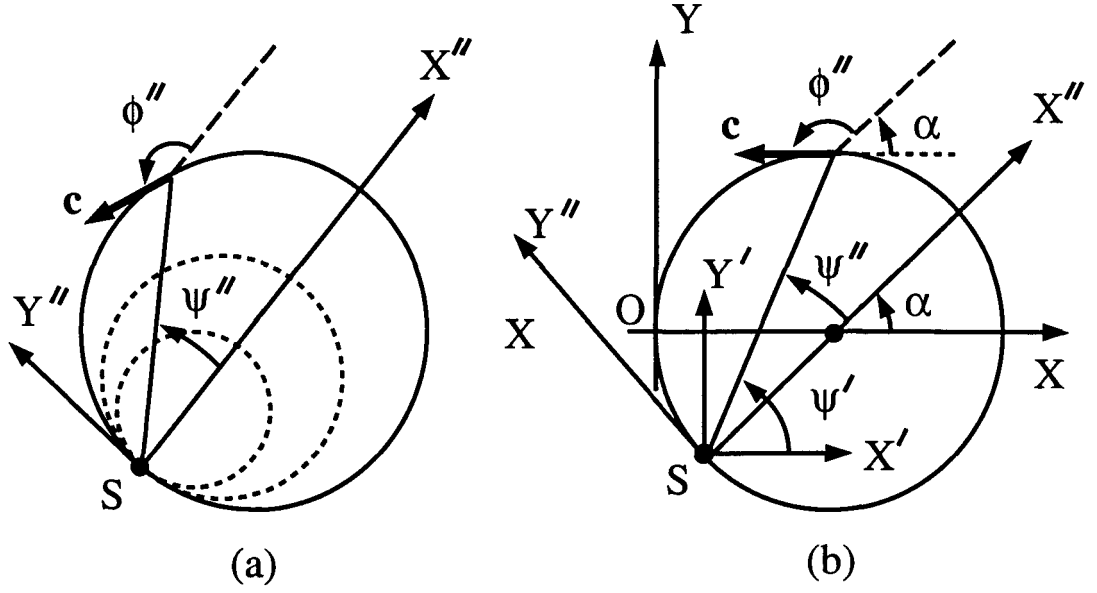$$K \left[\nabla^2 \phi - 4\cos\phi \, \nabla_x \nabla_z \phi - 4\sin\phi \, \nabla_y \nabla_z \phi \right.$$

Figure 3.2: Definition of the coordinate system and the angles used in the theoretical description of the structure of the domain.

$$+2(\sin \phi \ \nabla_x \phi - \cos \phi \ \nabla_y \phi) \ \nabla_z \phi] \quad = \quad 0 . \qquad (3.7)$$

Equation 3.7 is highly non-linear and seems intractable analytically. We, therefore, analyse the stability of the chiral domains by assuming an ansatz for $\phi(x, y, z)$.

From the experimental studies it is clear that the c-field within each layer is like part of a $+2$ disclination (Fig. **3.1a**). The structure rotates from layer to layer such that the locus of the singular point describes a helical line of period $2\pi/q$ (Fig. 3.1b). This structure can be modelled as follows: The local coordinate systems (X'', Y'', Z'') and (X', Y', Z') have their origins at the singular point, S, and co-rotate with the singularity. The former is rotated by an angle $\alpha = qz$ with respect to the latter which is parallel to the lab-fixed (X, Y, Z) system (Fig. 3.2). The $+2$ structure can then be described as

$$\phi''(x'', y'', z'') \quad = \quad 2\psi'' \pm \pi/2 , \qquad (3.8)$$

where the sign of the $\pi/2$ term defines the sense of rotation of the c-field. A negative(positive) sign of the $\pi/2$ term leads to a clock-wise(anti-clock-wise) sense of

the c-field *within* each layer; Fig. 3.1 corresponds to the negative sign. In a local (X', Y', Z') system (Fig. 3.2), which is parallel to the lab-fixed x, y, z system, with $\psi' = \arctan(y^l/x')$ and $a = qz$, the angle made by the c-vector with respect to the XI-axis is

$$
\begin{aligned}
\phi'(x', y', z') &= \phi'' + a \\
&= 2\psi' - \alpha \pm \pi/2 \\
&= 2\arctan(y^l/x^l) - qz \pm \pi/2
\end{aligned}
\tag{3.9}
$$

Going to the lab-fixed coordinate system $\phi(x, y, z)$ can be written as

$$
\phi(x, y, z) = 2\arctan\left[\frac{y + R\sin(qz)}{x - R\{1 - \cos(qz)\}}\right] - qz \pm \frac{\pi}{2},
\tag{3.10}
$$

where R is the radius of the domain. The handedness of the helical structure depends on the sign of q. Fig. **3.1b** corresponds to negative q. The elastic energy density diverges as the singularity is approached. Due to this reason, a core region (of radius $\rho_c \sim 100\text{\AA}$) around the singularity will be 'melted' and is a natural cut-off while performing the integration. It is convenient to choose a local polar coordinate system (Fig. 3.3) such that

$$
x' = \rho\cos\psi', \quad y' = \rho\sin\psi', \quad z^l = z
\tag{3.11}
$$

and

$$
\delta = \psi' - qz .
\tag{3.12}
$$

The free energy density, **Eq.** 3.4, becomes

$$
\begin{aligned}
f_{el}^{SmC} &= 2\left[K + (K_t Rq - 2K_{bt})Rq\cos^2\delta\right]\frac{1}{\rho^2} \\
&\quad -2\left[(K_t Rq^2 - K_{bt}q)\cos\delta\right]\frac{1}{\rho} + \frac{K_t}{2}q^2 .
\end{aligned}
\tag{3.13}
$$

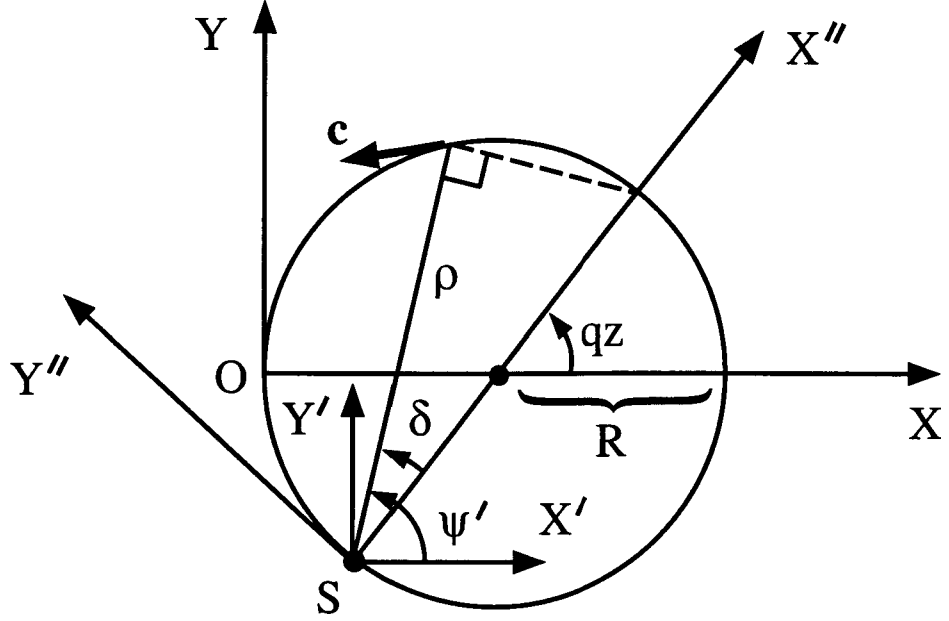The energy per unit length of the domain, neglecting the energy cost for creating

Figure **3.3**: Definition of the polar coordinate system used in the calculations.

the 'molten' core of the disclination line, can be obtained as

$$\frac{F_{el}^{SmC}}{L} = \int_0^1 dz \int_{qz-\pi/2}^{qz+\pi/2} d\psi' \int_{\rho_c}^{2R\cos\delta} \rho \, d\rho \, f_{el}^{SmC} \,, \tag{3.14}$$

where ρ_c is the cut off length. Thus the elastic free energy per unit length of the cylindrical domain can be obtained as

$$
\begin{aligned}
\frac{F_{el}^{SmC}}{L} = \quad & 2\pi K \ln\left(\frac{R}{\rho_c}\right) \mp 2\pi K_{bt} R q \left[\ln\left(\frac{R}{\rho_c}\right) + \frac{\rho_c}{R} - \frac{1}{2}\right] \\
& + \pi K_t R^2 q^2 \left[\ln\left(\frac{R}{\rho_c}\right) + \frac{4\rho_c}{R} - 1\right] \tag{3.15} \\
\simeq \quad & 2\pi K \ln\left(\frac{R}{\rho_c}\right) \mp 2\pi K_{bt} R q \left[\ln\left(\frac{R}{\rho_c}\right) - \frac{1}{2}\right] \\
& + \pi K_t R^2 q^2 \left[\ln\left(\frac{R}{\rho_c}\right) - 1\right] \,, \tag{3.16}
\end{aligned}
$$

since $\rho_c \ll R$. Equation **3.16** has a minimum for

$$q_0 \simeq \pm \frac{K_{bt}}{K_t R} \left[\frac{\ln\left(R/\rho_c\right) - 1/2}{\ln\left(R/\rho_c\right) - 1}\right] \,, \tag{3.17}$$
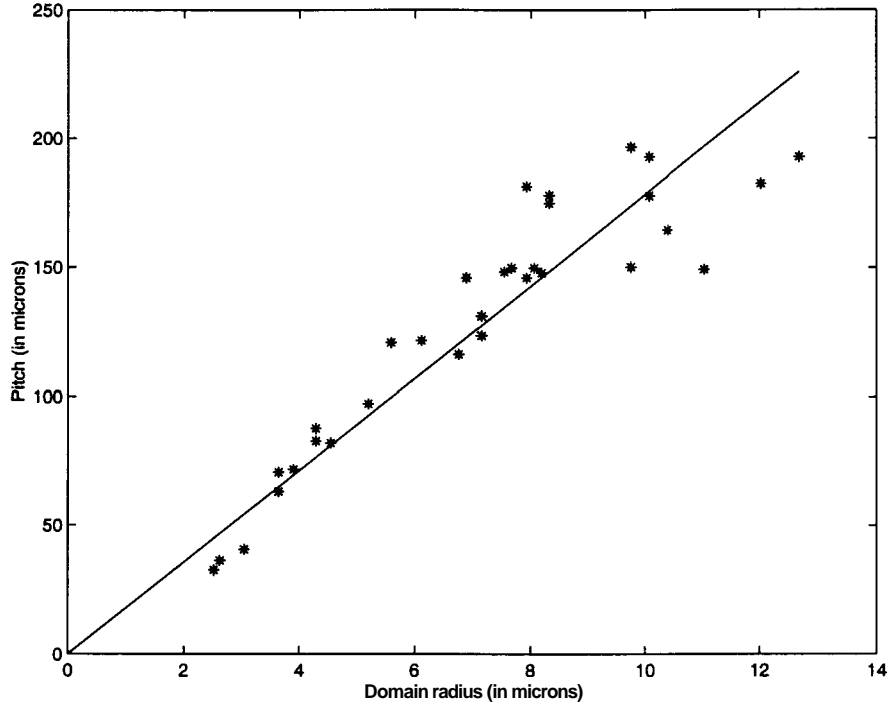
Figure **3.4:** Variation of the pitch of the helical band as a function of the radius of the domains. The experimental points (*) were obtained using cells of different thicknesses. The solid line is the theoretical fit obtained using **Eq. 3.17.**

where terms of order ρ_c/R and higher have been ignored and the sign on the r.h.s. of **Eq. 3.17** corresponds to that of the $\pi/2$ term in **Eq. 3.10.** It is clear that a nonzero K_{bt} implies an elastic free energy minimum for a nonzero value of q. From Eqs. **3.10** and **(3.16)** it follows that for a given sign of the bend in the c-field the sign of q_m is determined by that of K_{bt}. For $K_{bt} > 0$ the disclination line has the same sense of winding as the $\hat{n}$-field on the surface of the domain, and for $K_{bt} < 0$ the two have opposite senses. From the observations on the domains formed in the twisted nematic cells, we infer that K_{bt} is positive for this system.

A plot of the theoretical fit to the experimental values of the pitch as a function of the domain radius is shown in Fig. **3.4.** Assuming $q_o \simeq K_{bt}/K_t R$, the ratio K_{bt}/K_t is estimated to be **0.35.**

Thus we see that the system prefers a chiral structure for the domains even though the achiral system does not permit chiral terms in the free energy expression.

contribution from the tips is negligible compared to that from the 'cylindrical' portion of the helical structure described earlier.. The electric field experiments indicate that the chiral structure is preferred even in domains which are a few hundred microns long. We feel that the observed bent c-field configuration may be preferred due to the reasons stated below.

(i) An orderelectric polarisation near the interface: The orientational order parameter Q can be expected to vary sharply over a coherence length ξ (typically a few molecular lengths) at the N-SmC interface. This gives rise to an orderelectric polarisation

$$|\mathbf{P}_o| \sim e\,(\delta Q)/\xi\,, \tag{3.18}$$

where e is the relevant coupling coefficient, and an electric field

$$\mathbf{E} = (4\pi/\epsilon)\mathbf{P}_o \tag{3.19}$$

normal to the interface, where ϵ is the appropriate dielectric constant [38]. The bend distortion in the c-field generates a flexoelectric polarisation

$$|\mathbf{P}_f| \sim e/R\,, \tag{3.20}$$

where R is the radius of the cylinder and for simplicity we have used the same coefficient e. If the mutual orientation between E and $\mathbf{P}_f$ is favourable, the gain in energy per unit length of the cylinder

$$F_{elec} \sim \left(\frac{e}{R}\right)\left(\frac{e\,\delta Q}{\xi}\right)\left(\frac{4\pi}{\epsilon}\right)2\pi R\xi \tag{3.21}$$

The bend distortion costs an energy per unit length is

$$F_{bend} \sim \pi K \ln\left(\frac{R}{r_c}\right)\,, \tag{3.22}$$

where K is an elastic constant and r_c the core radius. Using the values (in cgs units) $e \sim 5 \times 10^{-4}, \delta Q \sim 0.1, \epsilon \sim 5$ and $K \sim 0.3 \times 10^{-7}$ for the c-vector distortions, there is a net gain in energy up to $R \sim 1\mu m$ if the c-field has a bend distortion.

(ii) An elastic coupling of the c-field to the concentration gradient in the binary mixture: In the two-component system the gradient of the concentration χ across the interface can be large. This can favour a bent c-field configuration at the surface. The surface-like term

$$F_{conc} = \kappa \int d\,V\; \mathbf{V} \cdot [\mathbf{c} \times (\boldsymbol{\nabla}\chi \times \mathbf{c})] = \kappa \int d\,S \cdot [\mathbf{c} \times (\boldsymbol{\nabla}\chi \times \mathbf{c})] \qquad (3.23)$$

in the elastic free energy is of particular interest. A negative value for κ favours the bent c-field configuration at the N-SmC boundary. Note that $\boldsymbol{\nabla}\chi$ can also contribute to $\mathbf{P}_o$ discussed above.

It should be noted that the boundary alignment with the c-vector tangential to the interface is compatible with a structure consisting of a straight +1 disclination line running along the domain axis (Fig. 3.6a). Such a configuration, which can be expressed as

$$\phi = \tan^{-1}\left(\frac{y}{x}\right) + \frac{\pi}{2}\,, \qquad (3.24)$$

is a solution to the Euler-Lagrange equation obtained from Eq. 3.4. The energy per unit length for a domain with a +1 line can be easily obtained as

$$\frac{F_{el}^{(+1)}}{L} = \pi K ln\left(\frac{R}{\rho_c}\right) + \epsilon_{core}\,, \qquad (3.25)$$

where ρ_c is the radius of the core of the defect and ϵ_{core} is the energy cost for creating the core. This is lower than that for the structure with a helical line running along the surface which is given by Eq. 3.16. As pointed out by Langer and Sethna for the $2D$ case [31], the advantage of having the +2-like structure with the core near the periphery over the +1 is that in the former case the defect core can be expelled from the domain by violating the boundary alignment over a small region (Fig. 3.6b). This would, of course, cost surface free energy which is always finite. Since the elastic energy density diverges logarithmically as the defect core is approached, expelling the defect by even a small amount can result in considerable reduction in the distortion free energy [31].
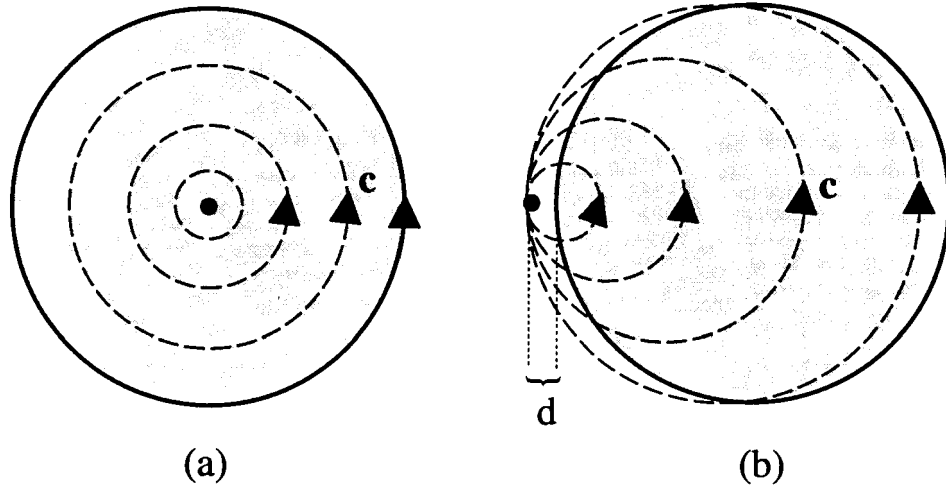
Figure 3.6: (a) The c-field in a *SmC* layer with a +1 disclination line. (b) A *SmC* layer (shaded region) where the defect core is 'expelled' from the layer by violating the boundary alignment condition. This costs additional surface energy but at the same time reduces the bulk elastic energy.

Apart from the above possibilities, the boundary alignment of ñ could also have led to a 'bâtonnet' structure which includes a focal-conic domain. Unlike in Sm A, the focal-conic structure in *SmC* is 'broken' and costs additional energy [23]. Moreover, the preferred boundary alignment condition (director parallel to the interface) is violated over a larger area in'the case of bâtonnets, compared to the other structures discussed above (see Fig. 2.1).

3.4 Stability of a +2 disclination line

Since the defect structure within each layer of the chiral domains is like part of a +2 disclination, it is interesting to see the effect of the bend-twist coupling on the stability of a full +2 line in *SmC* . The symmetry of the +2 structure allows us to restrict our attention to a case where the line stays in the YZ plane and is allowed to tilt in the direction of the Y axis (Fig. 3.7) by an angle β. The smectic layers are parallel to the XY plane. This structure can be described as

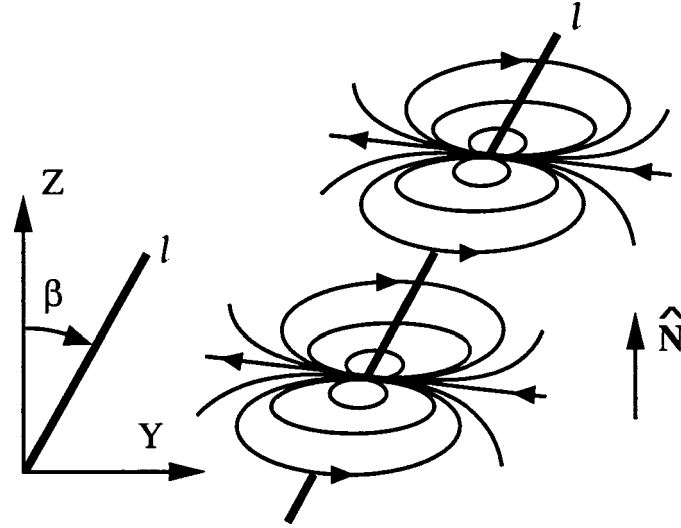$$\phi = 2\tan^{-1}\left(\frac{y - \alpha z}{x}\right) + \frac{\pi}{2} , \tag{3.26}$$

Figure 3.7: A schematic diagram showing a +2 disclination line l which is tilted by an angle β in the ZY-plane, with respect to the SmC layer normal.

where a $= \tan\beta$. We put x $= x' = \rho\cos\psi$ and y $- \alpha z = y' = \rho\sin\psi$ so that $\phi = \psi + \pi/2$.

From Eq. 3.4, the elastic free energy density for such a structure can be written as

$$f_{el}^{(+2)} = 2\left[K + K_t\alpha^2\cos^2\psi + 4K_{bt}\alpha\cos^2\psi\right]\frac{1}{\rho^2}. \tag{3.27}$$

Equation 3.27 has to be integrated over unit length of a cylindrical volume with the defect line as the cylinder axis. The intersection of a plane parallel to the X-Y plane with the cylinder of radius R is an ellipse of the form $x'^2/a^2 + y'^2/b^2 = 1$, where a $=$ R and b $= R/\cos\beta$ (Fig. 3.8). After integrating over ρ and z, the ψ integration was done numerically (using Gaussian Quadrature method [39]). With the following values (in CGS units): K $= K_t = 0.5$ x 10^{-6}, $K_{bt} = 0.1$ x 10^{-6}, $\rho_c = 1 \times 10^{-6}$ and R $= 5$ x 10^{-4}, the integrated energy has a minimum for $\beta = 35°$. A similar analysis done for a +1 line shows that the line prefers to be along the layer normal (no tilt).
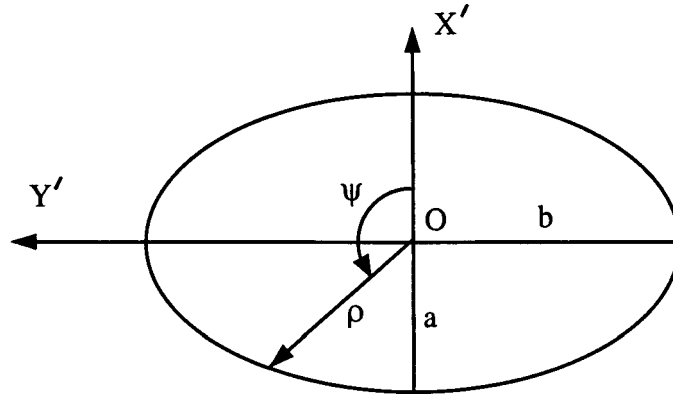
Figure 3.8: The elliptical section made by the intersection of a cylinder, whose axis is along the disclination line, with a plane parallel to the smectic layers.

3.5 Distortion energy for the nematic medium

From the experiments it is clear that the nematic surrounding the domain has a twist distortion. At the surface of the domain, the nematic director, $\hat{\mathbf{n}}$, lies in the tangent plane and is tilted with respect to the domain axis. This angle is roughly equal to the SmC tilt angle, θ_0, at the given temperature. At the cell walls the director is forced to lie along the alignment direction. These boundary conditions are satisfied by having a continuous twist deformation in the nematic director field surrounding the domain. For simplicity, we assume that the distortion is cylindrically symmetric with the twist angle changing from θ_0 to zero over a distance $(R_0 - R)$, where $2R_0$ is the cell thickness and R is the domain radius (Fig. 3.9). The director distribution can be represented as

$$\hat{\mathbf{n}} \equiv (n_r, n_\phi, \mathrm{n},) \equiv (0, \sin\theta, \cos 0) . \tag{3.28}$$

The Frank-elastic energy expression, with the usual one elastic constant approximation, can be written as

$$f_{el}^{nem} = \frac{K_n}{2} \left[(\nabla \cdot \hat{\mathbf{n}})^2 + (\nabla \times \hat{\mathbf{n}})^2 \right] . \tag{3.29}$$
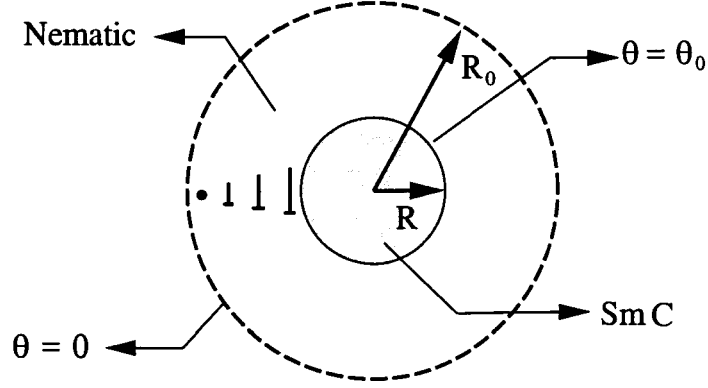
Figure **3.9:** Schematic representation of the nematic distortion around a SmC domain. The shaded region represent the cross-section of the SmC domain. The nails represent the projection of the Frank-director in the nematic.

In polar coordinates,

$$f_{el}^{nem} = \frac{K_n}{2} \left[\left(\frac{\partial \theta}{\partial r} \right)^2 + \frac{\sin^2 \theta}{r^2} + \frac{\sin(2\theta)}{r} \frac{\partial \theta}{\partial r} \right]. \tag{3.30}$$

The Euler-Lagrange equation obtained from **3.30** is

$$\frac{d}{dr} \left(r \frac{\partial \theta}{\partial r} \right) - \frac{1}{2r} \sin(2\theta) = 0 \tag{3.31}$$

and the boundary conditions are $8 = \theta_0$ at $r = R$ and $8 = 0$ at $r = R_0$. Eq. **3.31** can be integrated assuming 8 to be small (so that $\sin 8 \simeq 8$) to obtain the relation

$$\theta = \frac{\theta_0 R}{(R^2 - R_0^2)} \left(r - \frac{R_0^2}{r} \right) \tag{3.32}$$

Substituting **3.32** in **3.30** and integrating from $r = R$ to $r = R_0$, we get the nematic elastic free energy per unit length along the domain axis as

$$\frac{F_{el}^{nem}}{L} = 2\pi K_n \theta_o^2 \left[\frac{R^2}{(R_o^2 - R^2)} \right], \tag{3.33}$$

where K_n is the Frank-elastic constant of the nematic. Note that the distortion energy due to the nematic diverges as $R \to R_0$. This is because as the domain radius increases, the nematic director has to twist by θ_0 within shorter and shorter lengths. As we shall see in the next section, this distortion has a very significant role in deciding the equilibrium shape of the SmC domains.
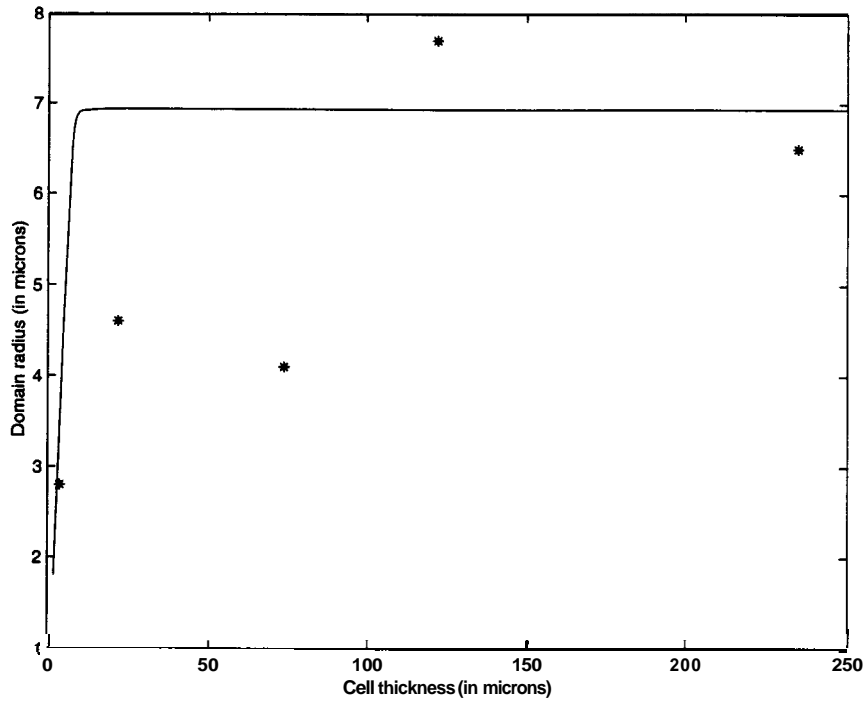
Figure *3.10:* Dependence of the radius of the domains on the cell thickness $(2R_o)$. The solid line is the theoretical curve obtained for the parameters given in the text. The *'s are the experimental data obtained from cells of different thicknesses. Each point is an average over several domains in a given cell.

3.6 Domain-shape analysis

In order to find the equilibrium shape of the domain we have to minimise the total free energy

$$F = F_{el}^{SmC} + F_{el}^{nem} + F_{surf} , \qquad (3.34)$$

where the first two terms are the elastic distortion energies for the SmC domain and the surrounding nematic given by Eqs. *3.16* and *3.33,* respectively. The third term is the surface energy contribution from the N-SmC interface. As before, we assume the domains to be perfect cylinders with flat ends. The interfacial energy can then be written as

$$F_{surf} = \gamma_{\parallel} 2\pi R L + \gamma_{\perp} 2\pi R^2 , \qquad (3.35)$$

where $\gamma_{\parallel}$ and $\gamma_{\perp}$ are the interfacial tensions for interfaces which are parallel and perpendicular to the cylinder axis, respectively and L, the length of the cylinder. Equation *3.34* has to be minimised at constant volume. This constraint gives the

the SmC domains the director makes a constant angle θ_o with the layer normal, N, which is along the Z-axis. As before, we assume that the domain is cylindrical. The variation in ϕ is described by **Eq.** 3.10. In the nematic medium, the director is taken to be parallel to the Z-axis at the two parallel glass surfaces of the cell. At the surface of the domain the Frank-director in the nematic and that in the SmC are parallel to each other. The variation of θ and ϕ in the nematic between the glass plates and the domain is assumed to be linear along the Y-axis.

A plane wave is assumed to be incident on the cell after passing through a polariser. The cell is oriented such that the alignment direction and hence the long-axis of the domain is parallel to the electric vector of the incoming polarised light. Since there are distortions in the director along the propagation direction, inside the cell the light is, in general, elliptically polarised. This polarisation state can be decomposed into two linearly polarised states which have their polarisation vectors orthogonal to each other. These are called the ordinary and the extraordinary states and they, in general, travel with different velocities given by the refractive indices n_o and n_{eff}, respectively.

Since the director-fields in the nematic and in the SmC domain are inhomogeneous both along the propagation direction and in the perpendicular planes, we divide the entire medium into cubic cells of constant volume. The dimension of a cell is chosen such that the director field within it can be assumed to be uniform. Since the principal refractive indices of the nematic and the SmC are comparable, we assume the same values of n_o (ordinary) and n_e (extraordinary) for both the media. This allows us to neglect effects like reflection and refraction at the N-SmC interface. Also, since the birefringence, $(n_e - \text{n,})$ $\ll$ n, or n,, refraction within a medium can be ignored wherever the gradients in the director-field are small. However, the refraction effects might be considerable very close to the singular line, near which there are sharp variations in the director-field and hence in the effective refractive
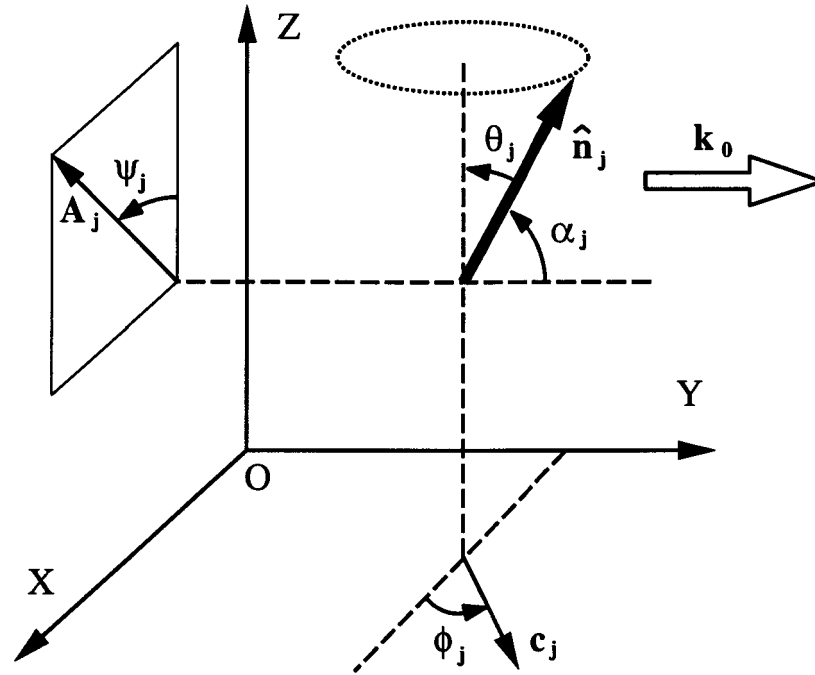
Figure **3.12:** Diagram showing the different angles described in the text.

---

index, n_{eff}. For the sake of simplicity, we have ignored these effects in calculating the transmitted intensities. In the simulation the incident plane wave after passing through the polariser P_1 has its wave-vector, k_0, along the Y-axis and the elecrtic-vector parallel to the Z-axis. The analyser is set such that this polarisation state is completely extinguished.

3.7.1 The 2 x 2 matrix method

In order to calculate the transmitted intensity, we make use of the **2** x **2** matrix method [40, 41]. In this method, a one dimensionally inhomogeneous, birefringent medium is assumed to be made up of a stack of perfectly homogeneous birefringent plates along the ray propagation direction. When a plane wave passes through such a system, there is a phase difference introduced between the ordinary and the extraordinary rays on passing through each plate and a rotation of the polarisation vectors (index ellipsoid) on going from one plate to another. The rotation is due to the twist distortion in the director along the propagation direction of the wave.

The values of each of these effects depend on the orientations of the optic axes of the plates as well as on the two refractive indices, n_e and n_o, of the medium.

The rotation of the polarisation vectors and the path difference introduced can be expressed in the form of matrices $\mathbf{R}$ and $\mathbf{S}$, respectively. If the wave-vector, $\mathbf{k_0}$, of the incident plane wave is taken to be along the Y-axis, the rotation introduced on passing from the $(j-1)^{th}$ plate to the jth plate is

$$\mathbf{R}_j = \begin{pmatrix} \cos(\psi_j - \psi_{j-1}) & \sin(\psi_j - \psi_{j-1}) \\ -\sin(\psi_j - \psi_{j-1}) & \cos(\psi_j - \psi_{j-1}) \end{pmatrix},$$

where ψ_j is the angle made by the projection of the optic axis (or the director in our case) on to the XZ-plane, as measured from the Z-axis (see Fig. 3.12). More precisely, the rotation matrix $\mathbf{R}$ performs the transformation of the polarisation vectors from the frame determined by the optic axis in the $(j-1)^{th}$ plate to the jth plate. The path difference introduced between the ordinary and the extraordinary rays by the jth plate of thickness $\triangle y$ is given by

$$\mathbf{S}_j = \begin{pmatrix} e^{in_o 2\pi \triangle y/\lambda} & 0 \\ 0 & e^{in_{eff} 2\pi \triangle y/\lambda} \end{pmatrix},$$

where λ is the wave-length of light. The value of n_{eff}, which is the effective refractive index, is given by the expression

$$n_{eff} = \frac{n_o n_e}{\left[n_o^2 \sin^2 \alpha_j + n_e^2 \cos^2 \alpha_j\right]^{1/2}}, \tag{3.37}$$

where α_j is the angle made by the director with respect to the propagation direction, $\mathbf{k_0}$. The orientation of the director in the jth cell can be described using the angles θ_j and ϕ_j as $\hat{\mathbf{n}} \equiv (\sin\theta_j \cos\phi_j, \; \sin\theta_j \sin\phi_j, \; \cos\theta_j)$ The angles α_j and ψ_j can be related to θ_j and ϕ_j as (see Fig. 3.12)

$$\cos\alpha_j = \sin\theta_j \sin\phi_j \tag{3.38}$$

$$\sin\psi_j = \frac{(\hat{\mathbf{k}} \times \mathbf{A}_j) \cdot \hat{\mathbf{j}}}{|\mathbf{A}_j|}$$

$$= \frac{\sin\theta_j \cos\phi_j}{\sin\alpha_j} \tag{3.39}$$

Figure **3.13:** Simulated texture of half a pitch of the chiral domain. Only quarter pitch was simulated at a time for computational convenience. The vertical line is due to this reason.

The output state E_o is obtained from the input state E_i through the relation

$$E_o = P_2 R_{N+1} \left(\prod_{j=1 \to N} S_j R_j \right) P_1 E_i , \qquad (3.40)$$

where P_1 and P_2 are matrices representing the polariser and the analyser, respectively. The matrix R_{N+1} is the reverse transformation matrix to bring the system back to the lab-fixed frame.

3.7.2 Results

The simulated optical texture of a section of the helical domain is shown in Fig. **3.13.** The texture shows a dark band running close to the disclination which appears as a highly distorted line. This texture resembles the experimentally observed patterns shown in Fig. 2.4, which was recorded using white light. In the simulation the disclination line was assumed to be running on the surface of the domain. In the actual domains this line may be expelled from the domain as was discussed earlier. This might smoothen out the pattern very close to the disclination line.

3.8   Conclusion

We have theoretically analysed the stability of the chiral domain structures described in the previous chapter. This analysis shows that the helical structure is due to a cross coupling between the bend and *twist* deformations in the c-vector field. This is the first demonstration of the effect of such a coupling which is allowed by the symmetries of the smectic-C liquid crystal. By comparing the theoretical results with the experiments, we were able to determine the ratio of the elastic constants K_{bt}/K_t.

An analysis of the twist deformation produced in the nematic shows that the energy cost for this deformation restricts the radial growth of the domains in thin cells. The unusual shape of these domains is due to this and the anisotropic nature of the N-SmC interfacial tension.

We have also simulated the optical texture exhibited by the chiral domains and the results agree reasonably well with the experiments.